On the electrical and optical characteristics of reverse-biased silicon p-n junctions embedded in a metal-oxide-semiconductor field-effect-transistor device

KAIKAI XU[a,b*], HAITAO LIU[a], QI YU[b], ZHIYU WEN[a], GUANNPYNG LI[c]

[a]*Defense Key Disciplines Lab of Novel Micro-nano Devices and System Technology, Chongqing University, Chongqing, China 400044*

[b]*State Key Laboratory of Electronic Thin Films and Integrated Devices, University of Electronic Science and Technology of China, Chengdu, Sichuan, China 610054*

[c]*California Institute for Telecommunications and Information Technology, Irvine, CA 92697*

In this paper, we discuss the emission of visible light by a monolithically integrated silicon metal-oxide-semiconductor field-effect-transistor (Si-MOSFET) in which the p-n junctions are reverse-biased. The emission of light is observed from reverse-biased p-n junction though silicon is an indirect bandgap material. In this paper new research results with regard to two- and three- terminal Si-LEDs in the p-type MOSFET device are presented. Light emission from the two devices types (1) silicon p-n junction diode (2) silicon p-n junction gate-controlled diode with the junction biased in controlled avalanche breakdown. A multi-mechanism model fitting measured spectra is presented and justified, with the conclusion that the dominant light-emission mechanism is due to a combination of avalanche breakdown and tunneling.

(Received July 16, 2015; accepted October 28, 2015)

Keywords: Emission, Silicon, Spectral analysis, Transistors

1. Introduction

Silicon photonics is the "technology of making optical devices using silicon and standard CMOS manufacturing techniques". Although silicon is the most widely used semiconductor for building integrated circuits, including microprocessor, it is not common to make silicon photonic devices, such as light sources and modulators [1].

Although silicon is an indirect bandgap material in which non-radiative process such as free carrier absorption and Auger recombination dominates, light emission from reverse-biased p-n junctions was reported for the first time in 1955 [2]. Since electro-hole pairs are produced during avalanche breakdown, some radiative recombination occurs. Both the electrons and the holes can be heated by the electric field. The radiative transition between hot carriers emits photons larger than the energy gap. Hence, the luminescence during avalanche breakdown is characterized by a broad emission spectrum. This spectrum extends to $h\nu = 3E_g$ which represents the energy separating the hottest electron from the hottest hole (recall that the energy for impact ionization by a hot carrier is about $1.5E_g$); on the other hand, the low-energy edge of the emission spectrum extends to energies lower than the gap energy, due to the tunneling-assisted photon emission [3].

In recent years, several technologies utilizing single crystal silicon junctions as practical light emitting diodes have been proposed, but these technologies make use of non-standard silicon IC technology. Silicon light-emitting devices (Si-LEDs) will only become practical if they can be fully integrated with relevant silicon integrated circuits, using standard IC technology. Accordingly, we have decided to investigate the design and properties of silicon light emitting devices fabricated by conventional CMOS IC technology [4].

The avalanche light emitting devices exhibited properties similar to experimental results reported in [5], with the main characteristics being: (1) a linear light intensity vs. reverse current characteristic, and (2) no significant variation in the shape of the emission spectrum (400–900 nm) as the reverse current increases. In contrast to the two-terminal silicon p-n junction diode in which the light intensity is dependent on the avalanche current, a novel three-terminal silicon gate-controlled diode (MOS-like structures) is described where the light intensity of the device is controlled by an insulated MOS gate voltage [6],[7].

Indeed, a p-type MOS-like device (i.e., PMOSFET) is able to operate either as Si-diode LED or as Si gate-controlled diode LED [8],[9]. In this paper a review of our silicon electro-optic device is given, followed by new research results with regard to a multi-mechanism model fitting the measured spectrum is presented.

2. Experimental details

Standard 3μm CMOS process with self-aligned technology is utilized for fabrication. The starting wafer is an n-type <100> Si with resistance of 0.8–1.2 Ω•cm, thickness of 525 ± 25 μm, and diameter of 100 mm. Typical processes are introduced as follows. Well drive-in is done in the ambient of 1 hour N_2, 2 hours O_2, and 4 hours N_2 at the temperature of 1200℃ by implanting boron with dose 10^{13} cm^{-2} and energy 60 keV. In regard to ion implantation, for p ring, it is 3×10^{15} cm^{-2} with 80 keV; for n ring, it is 5×10^{15} cm^{-2} with 80 keV. for p^+ S/D, it is 3×10^{15} cm^{-2} with 80 keV; for n^+ S/D, it is 3×10^{15} cm^{-2} with 80 keV. Annealing is implemented at 850 ℃ for 30 minutes. A cross-section view of the PMOSFET device used for the analysis of the electrical and optical characteristics of reverse-biased silicon p-n junctions embedded in a metal-oxide-semiconductor field-effect-transistor device is shown in Fig. 1.

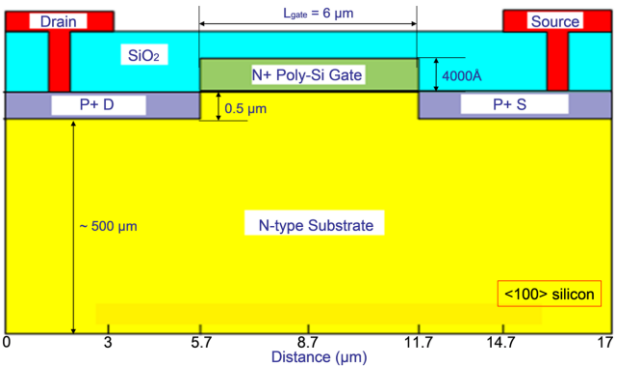

Fig. 1. Schematic illustration of the structure of PMOSFET

The presence of reverse current in the PMOSFET device can be detected using the experimental configuration shown in Fig. 1. In the case of two-terminal p-n junction diode, the gate terminal is floated with varying the junction's reverse-bias to make the junction avalanche breakdown, thus utilizing a p-n junction that operates in the reverse breakdown mode to realize a light emitting source; In the case of three-terminal gate-diode, the reverse-bias is fixed with varying the gate voltage, thus confining the light emitting zone close to the silicon surface in close proximity to transparent Si-SiO_2 layers.

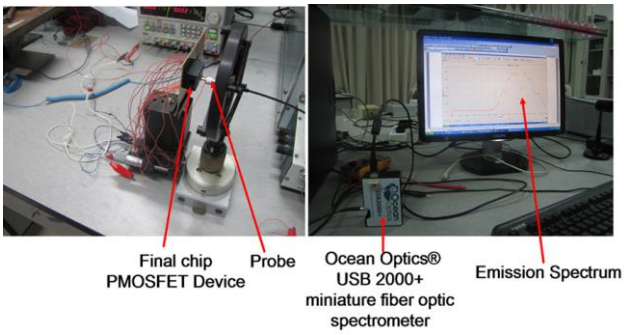

Fig. 2. Experimental setup for the light emission measurement

As shown in Fig. 2, the MOS-like device is electrically driven by either a programmable electrometer or a voltage source meter, the working distance between the focusing lens and the sample is fine-tuned to maximize the photoluminescence (PL) intensity. Calibrated CCD detector, which is responsive to 200 to 1100 nm, is positioned immediately above the device to collect most of the emitted light. The electroluminescence (EL) ranged from 400 to 900 nm is detected by a charged-coupled device (CCD)-based spectrum (Ocean Optics, USB-2000).

3. Results and discussion

3.1 Structural characteristics

In the present study, the light emission in silicon under reverse-biased condition has been explained on the basis of the theory of ionization and recombination of electrons and holes. The relative intensity of the emitted light has been calculated and the results correspond with the experimental results presented in [10], [11]. Several attempts have been made to understand the origin of emitted light observed from silicon p-n junction in avalanche breakdown. According to the properties of electron-hole avalanches in reverse-biased silicon junction, the physical mechanisms of the emission can be categorized by the following three types of process

- Indirect interband transitions of energetic electrons in the conduction and holes in the valence band [12]
- Indirect intraband transitions of energetic electrons in high field region near charged impurities. This

process is also known as Bremsstrahlung radiation [13]

- Direct [12], [13] and indirect [14] interband transition of hot electrons in the conduction band and hole in the valence band. This process consists of radiative and non-radiative electron-hole recombination

In practice, the emission of light results from radiative transition of the high-energy carriers produced by the breakdown of the junction related to local heating. In the avalanche breakdown process, free carriers are able to gain enough energy from the field between collisions for them to break covalent bond in the lattice when they collide with it. In this process, called avalanche breakdown, every carrier interacting with the lattice as described above creates two additional carriers. All three carriers can then participate in further avalanching collisions, leading to a sudden multiplication of carriers in the space-charge region when the maximum field becomes large enough to cause avalanche. The electron travels, on the average, a distance which is known as mean-free-path, before interacting with an atom in the lattice and losing energy. After that, the lost energy of electron will be transferred to a photon. As a result, the light is emitted in the reverse-biased breakdown of silicon from localized regions where the quantum dots (i.e., the immobile charged centers in the space-charge region) are. In order to calculate the intensity of emitted light against the energy of the photons, the classic Boltzmann equation is taken into consideration. Considering a volume V that contains N_α particles of a species α. The distribution function $f_a(\ell,\nu,t)$ gives the average number of particles dN_α which have the position $\ell \to \ell + d\ell$ and velocity $\nu \to \nu + d\nu$ at time t

$$f_\alpha(\ell,\nu,t) = \frac{dN_\alpha}{d\ell} d\nu \tag{1}$$

The particle density is given by

$$n_\alpha(\ell,t) = \int f_\alpha d\nu \tag{2}$$

The rate of change of the number of particle in a given element ($\ell \to \ell + d\ell$, $\nu \to \nu + d\nu$) in phase space is simply the difference between the rate at which particles enter and leave the element. With the assumption that the rate of change of f_α due to collisions is denoted by $\left(\frac{\partial f_\alpha}{\partial t}\right)_c$ and that the acceleration due to external forces by a. In the short interval $t \to t + dt$, the changes at (ℓ,ν) will move to ($\ell + \nu$, Δt and $\nu + a$, Δt); all other changes in the orbit are bound up in the collision term and

$$f_\alpha(\ell + \nu\Delta t, \nu + a\Delta t; t + \Delta t) - f_\alpha(\ell,\nu,t) = \left(\frac{\partial f_\alpha}{\partial t}\right)_c \Delta t \tag{3}$$

The final distribution function may now be expanded about the initial value, and in the limit $\Delta t \to 0$, it yields

$$\frac{\partial f_\alpha}{\partial t} + \nu \cdot \frac{\partial f_\alpha}{\partial \ell} + a \cdot \frac{\partial f_\alpha}{\partial t} = \left(\frac{\partial f_\alpha}{\partial t}\right)_c \tag{4}$$

Integrating over t, Eq. (4) becomes

$$f(E) = C \exp\left(-\frac{E}{kT_e}\right) \tag{5}$$

where $f(E)$ is the energy distribution function of photon intensity, C is an empirical constant, k is the Boltzmann‘s constant, and T_e is the effective electron temperature which is related directly to the maximum electric field in the space-charge region [15]. Furthermore, the kinetic energy of electron is given by $kT_e = q\mathrm{E}\ell_m$, where q is the magnitude of elementary charge, E is the field in which electrons are being accelerated, and ℓ_m denotes the mean-free-path of electron.

Generally speaking, photons are generated by the interaction of carriers and ions with the immobile charged centers located in the space-charge region. As temperature decreases, the mean-free-path of electron-phonon interaction increases, thus reducing the probability of phonon scattering and leading to more energetic electron. Because of the increase in radiative recombination rate, the emitted light intensity increases. Accordingly, Eq. (5) presents the evidence that light intensity increases with temperature [16]. The theoretical results of the intensity of the emitted light in reverse-biased p-n junction are in good agreement with the reported experimental results [17].

In summary, emitting photons closely depend on the carriers induced by impact ionization. The similarity

between energy distribution function of photon intensity (shown in Eq. (5)) and energy distribution function of carrier (i.e., the lucky-electron model being used to characterize the hot-carrier effect [18]) exhibits the fact that avalanche current (i.e., the reverse current in the p-n junction) is linear with the light intensity. Effective temperature T_e being directly determined by the electric field E in the depletion region implies that E should be the major reason for light emission in the reverse-biased silicon p-n junctions.

3.2 Electrical properties

- Silicon-diode LED

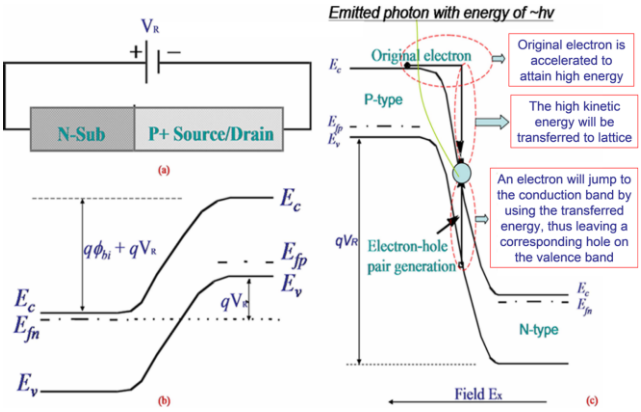

Fig. 3. One-half of the Si-PMOSFET LED: (a) Schematic diagram; (b) Energy-band diagram; (c) Impact ionization in which an energetic electron generates a new electron-hole pair.

The avalanche breakdown occurring in p-n junction diode in the Si-PMOSFET device is simply presented in both Fig. 3. The transition from soft breakdown to hard breakdown produces the evidence that a large excess reverse current, which is due to localized breakdown in small high-field regions around metallic precipitates present within the crystal, already flows through this diode at reverse voltages well below the avalanche breakdown voltage [19].

Since the threshold voltage V_t of the PMOSFET device is in the range -1.5 V to -2.0 V and the thickness of SiO_2 layer ranges from 400 to 500 Å, a detailed deduction based on the empirical threshold voltage formula is presented in Fig. 4. For a one-sided p^+ n abrupt-junction, the critical field for avalanche breakdown is given by

$$\mathrm{E}_{BR}(T)=\sqrt{\frac{2qN_d}{\varepsilon_{si}}\left[BV(T)\right]} \tag{6}$$

where q is the elementary charge, N_d is the background doping concentration, and ε_{si} is the permittivity of silicon. Assuming that the electric field is a fixed value and the impact ionization rate is taken into consideration, the breakdown voltage at room temperature can be approximately expressed as

$$BV=60\left(\frac{E_g}{1.1}\right)^{1.5}\left(\frac{N_d}{10^{16}}\right)^{-0.75} \tag{7}$$

Since N_d is the doping concentration at the surface of the n-type substrate of the Si-PMOSFET device, the *BV* of this one-side abrupt p-n junction (i.e., "P^+ Source/Drain" to "N-Substrate" junction) with the background doping concentration of $2.5\times10^{16}\mathrm{cm}^{-3}$ at the surface is accordingly equal to 30 V.

$$V_t=V_{fb}+2\phi_f-\frac{\varepsilon_{si}}{\varepsilon_{ox}}t_{ox}\sqrt{\frac{4qN_d}{\varepsilon_{si}\varepsilon_0}\left(-\phi_f\right)}$$

For n-type substrate with the doping concentration of 2.5×10^{16} cm^{-3}, Buck potential:

$$\phi_f=-\left(\frac{kT}{q}\right)\ln\left(\frac{N_d}{n_i}\right)=-(0.026)\ln\left(\frac{2.5\times10^{16}}{9.65\times10^{9}}\right)\approx-0.384V$$

Background doping concentration

Surface potential of substrate at threshold:

$$\phi_s=2\phi_f\approx-0.768V$$

Voltage drop across SiO_2 layer:

$$V_{ox}=-\frac{Q_{ox}}{C_{ox}}=-\frac{\varepsilon_{si}}{\varepsilon_{ox}}t_{ox}\sqrt{\frac{4qN_d}{\varepsilon_{si}\varepsilon_0}\left(-\phi_f\right)}=-\frac{11.8}{3.9}t_{ox}\sqrt{\frac{4\times(1.6\times10^{19})\times(2.5\times10^{16})}{11.8\times8.854\times10^{-14}}\times0.384}$$

Flat-band voltage:

$$V_{fb}=-\left(\frac{E_g}{2q}+\phi_f\right)=-(0.56-0.384)=-0.176V$$

For

$$t_{ox}=400\times10^{-8}cm$$

$$V_t=(-0.176)+(-0.768)+(-0.928)=-1.872V$$

For

$$t_{ox}=500\times10^{-8}cm$$

$$V_t=(-0.176)+(-0.768)+(-1.16)=-2.104V$$

Calculated range of threshold voltage V_t

Fig. 4. Numerical calculations of breakdown voltage of the "P^+ Source/Drain to N-Substrate" junction

In regard to the electroluminescence, Fig. 5 presents

the optical properties observed in the Si-diode LED and experimental results measured from the Si-diode LED. It is concluded that the theoretical analysis above can correspond reasonably well with the results presented in Fig. 5. The emitted light intensity is directly proportional to the reverse current flowing through the p-n junctions. This proportionality provides the evidence that a single-particle process is responsible for photon emission, both in the high-energy tail and in the near band-gap region.

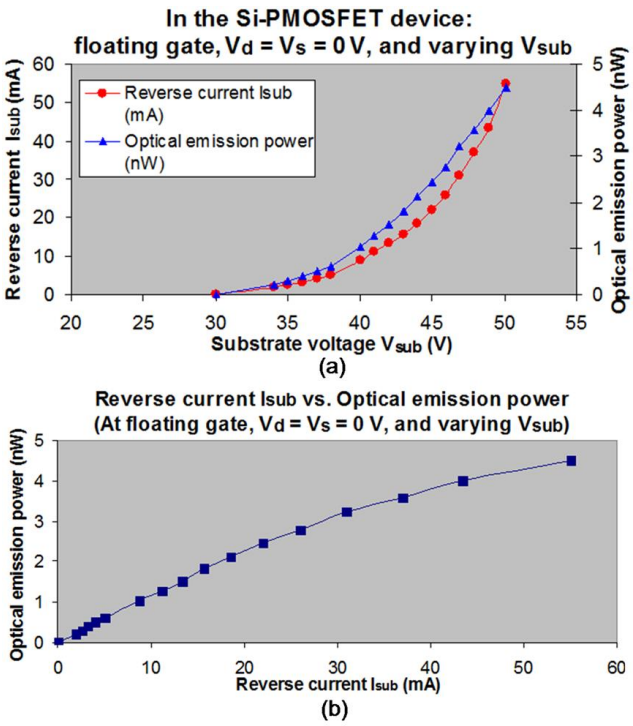

Fig. 5. In the case of Si-diode LED: (a) Correlation between the optical emission power and the avalanching reverse-current I_{sub} as a function of the substrate voltage V_{sub}, which is equivalent to the reverse bias of the "P^+ Source/Drain to N-Substrate" junction diode; (b) Relationship between the optical emission power and the reverse current

Furthermore, the Ref.[20] suggested that recombination between holes and electrons in the junction depletion layer should lead to dependence proportional to the square power of the avalanching reverse current, and that the only recombination process with intensity proportional to the reverse current should be the recombination between an avalanching carrier reaching the neutral region and a minority carrier.

Fig. 6 shows one of the typical broad-band photon emission spectra detected in the Si-PMOSFET device operating in the mode of silicon-diode LED. No significant shift in the spectrum is observed with different operating reverse-bias, and the spectrum shape is independent of the reverse current.

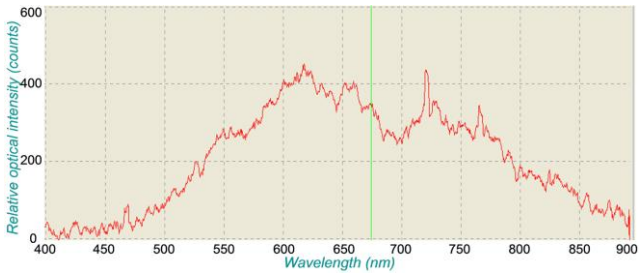

Fig. 6. Optical spectrum observed at V_{sub} = 48 V, V_d = V_s = 0 V, and floating gate. In this case, V_{sub} is equivalent to the reverse bias of the "P^+ Source/Drain to N-Substrate" junction diode

The similarity of the spectrum shape at different reverse currents could be explained as follows. When the p-n junction is reverse-biased above the breakdown voltage, the space charge due to the avalanche current lowers the junction electric field to the breakdown value. Despite the avalanching reverse-current increasing with the additional reverse-bias, the steady-state junction electric field is always at the breakdown value.

- Silicon gate-controlled diode LED

In contrast to the two-terminal Si-diode LED in which the control of the light emission intensity is performed via the injection of carriers into the avalanche region, a three-terminal Si gate-controlled-diode LED is described where the light intensity of the Si-PMOSFET device is controlled by an insulated MOS gate voltage.

In Si-diode LED, because the electric field in the depletion region and the reverse-current both increase with the reverse-bias voltage V_{sub}, reverse-bias of the p-n junctions is proportional to the light emission intensity. On the contrary, in silicon gate-controlled-diode LED, because the reverse-bias of the "P^+ Source/Drain to N-Substrate" junction is a fixed value that is equal to V_{sub} = 35 V, the increase in light emission intensity should be attributed to increasing the gate voltage.

The reverse bias of V_{sub} = 35 V is lower than the avalanche breakdown voltage *BV* of the "P^+ Source/Drain

to N-Substrate" junction at V_g = 0 V. In other words, there is no avalanche breakdown occurring at the reverse-bias of 35 V, which implies that the light emission observed in the gate-controlled-diode case is due to the function of V_g. In fact, V_g is increased to change the field distribution at the surface of the "P^+ Source/Drain to N-Substrate" junction, thus reducing the *BV* of the "P^+ Source/Drain to N-Substrate" junction.

Since the reverse bias V_{sub} of the "P^+ Source/Drain to N-Substrate" junction is a constant, the reverse-current I_{sub} flowing through the p-n junction is expected to increase with the gate voltage V_g. It has been experimentally demonstrated that reverse current I_{sub} is proportional to gate voltage V_g, as shown in Fig. 7.

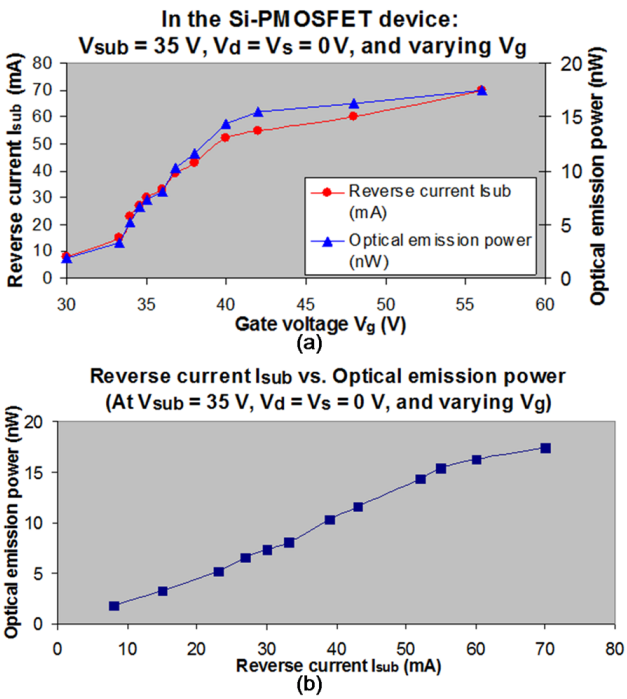

Fig. 7. In the case of Si gate-controlled-diode LED: (a) Correlation between the optical emission power and the avalanching reverse-current I_{sub} as a function of the gate voltage V_g while the reverse bias of the "P^+ Source/Drain to N-Substrate" junction is fixed to V_{sub} = 35 V; (b) Relationship between the optical emission power and the reverse current

The spectral characteristics at a fixed gate voltage V_g = 38 V are shown in Fig. 8 for the Si-PMOSFET device operating in the mode of gate-controlled-diode LED. No obvious shift in wavelength peaks is observed at different gate voltages.

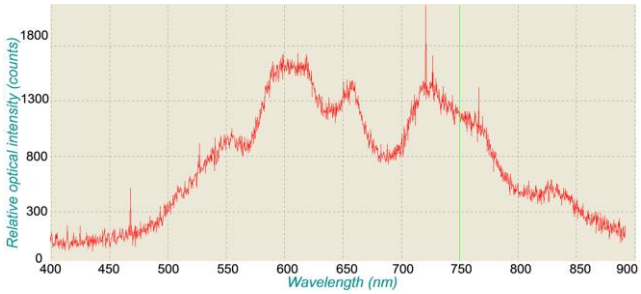

Fig. 8. Optical spectrum observed at V_{sub} = 35 V, V_d = V_s = 0 V, and V_g = 38 V. In this case, V_{sub} is equivalent to the reverse bias of the "P^+ Source/Drain to N-Substrate" junction. Gate voltage V_g is applied to make the Si-PMOSFET device be a Si gate-controlled diode LED

Since the light intensity could be modulated by the gate terminal [21] and the device is evaluated as an efficiency low voltage silicon CMOS light emitting device for electro-optical interface [22], the design and simulation of a three-terminal silicon thermo-optic modulator is presented to further indicate that the device has an intrinsic high-frequency operating capability into the near gigahertz range [23].

3.3 Optical properties

In order to calculate the light emission intensity for the various optical mechanisms mentioned above, the photon emission rate is given by

$$R = v\frac{C}{4\pi}\sum_{u,l}\int d\Omega_v \sum_{\lambda,k_u,k_l} M_\lambda(u,l,k_u,k_l,v) f_u(E_u(k_u)) \times f_l(E_l(k_l))\delta(E_f - E_i) \tag{8}$$

where $f(E_i(k))$ denotes the distribution function for electrons of band index i and wave vector k, parameters u and l indicate the upper and lower band indices for the transition of $\bar{f} = 1 - f$, respectively, v is the optical frequency, and C is a constant factor that is proportional to the product of the optical densities of state. Since Eq. (8) consists of both the direct transition rate and the indirect transition rate, the numerical expressions for the two rates above can be given by the following two equations

$$R_{direct}(v)=32vC\sum_{ul}\frac{V}{8\pi^3}\int_{RZ}d^3kf_u(E_u(k))\,\bar{f}_l(E_l(k))\sum_{i-1}^{3}\left|\langle u|\nabla_i|l\rangle\right|^2\delta(E_l(k)-E_u(k)+hv) \tag{9}$$

for spontaneous-emission rate for direct transition, and

$$R_{indirect}(v)=32vC\sum_{ul}\frac{V}{(8\pi^3)^2}\left(\int_{RZ}d^3k_lS_l(v,k_l)\int_{BV}d^3k_u+\int_{RZ}d^3k_uS_u(v,k_u)\int_{BZ}d^3k_u\right)\times\bar{f}_l(E_l(k_l))f_u(E_u(k_u))\left|\langle k_u|H_p|k_l\rangle\right|^2\delta_{if} \tag{10}$$

for indirect-photon-emission rate. Note that the parameters $\bar{f}_l$, S_n, and δ_{if} are given respectively by

$$\bar{f}_l(E_l(k_l))=1-f_l(E_l(k_l)) \tag{11}$$

$$S_n(v,k)=\sum_{i=1}^{3}\left|\sum_m\frac{\langle mk|\nabla_i|nk\rangle}{E_n(k)-E_m(k)-hv}\right|^2 \tag{12}$$

$$\delta_{if}=\delta(E_l(k_l)-E_u(k_u)+h(v+v_p))+\delta(E_l(k_l)-E_u(k_u)+h(v-v_p)) \tag{13}$$

According to the probability of electron-hole recombination under indirect transition and substituting the density of state that is closely related to the constant C, the indirect-photon-emission rate in Eq. (9) becomes

$$R(hv)=\frac{32\pi^3}{c^3h^4}n^2(hv)^2\left[hv\frac{dn}{d(hv)}+n\right]\times\int_{E_v}\int_{E_c}\exp\left[-\frac{(E_c-E_v-\Delta E)}{kT}\right]\times\sqrt{(-E_v)(E_c-E_g)}\times\delta(E_v-E_c+hv\pm k\theta)dE_cdE_v \tag{14}$$

where n is the refractive index of silicon, $\Delta E=E_{Fn}-E_{Fp}$ is the difference between the n-type semiconductor's quasi-Fermi level for electrons and the p-type semiconductor's quasi-Fermi level for holes, T is the lattice temperature, E_g is the energy band-gap, and $k\theta$ is the energy of phonon. The lower edge of the conduction band E_c designates the potential energy of an electron and the upper edge of the valence band E_v designates the potential energy of a hole. Solving Eq. (14) by integrating emission with absorption phenomena, the optical emission power per unit optical frequency in total can be expressed as

$$I_{relative}=I_{emission}-I_{absorption} \tag{15}$$

where

$$I(v)_{emission}\sim n^2(hv)^2(hv+k\theta-E_g)\times\exp\left[\frac{1}{k_0}(hv+k\theta)\left(\frac{1}{T_h}-1\right)+\frac{\Delta E}{T}-\frac{1}{2}(hv+k\theta-E_g)\left(\frac{1}{T_e}+\frac{1}{T_h}\right)\right]\times\frac{aI_1}{2}(hv+k\theta-E_g) \tag{16}$$

and

$$I(v)_{absorption}\sim n^2(hv)^2(hv-k\theta-E_g)\times\exp\left[\frac{1}{k_0}(hv-k\theta)\left(\frac{1}{T_h}-1\right)+\frac{\Delta E}{T}-\frac{1}{2}(hv-k\theta-E_g)\left(\frac{1}{T_e}+\frac{1}{T_h}\right)\right]\times\frac{aI_1}{2}(hv-k\theta-E_g) \tag{17}$$

where $k\theta=-\frac{1}{2}\left((hv)_{emission}-(hv)_{absorption}\right)$ is the energy of the phonon, and I_1 is the modified Bessel function of the order of 1. Moreover, k is the Boltzmann's constant and θ is the angle between the electric field (i.e., Coulomb field) and the electron/hole velocity. For θ, it is known that both the nuclear (i.e., the Coulomb charged centers or artificial atoms in the depletion region of p-n junction) and electron spin degrees of freedom in silicon nanostructures is able to be manipulated by the hyperfine interaction in which the electron transport in quantum dots is localized. Subsequently, if the Boltzmann approximation is applied, the hot-carrier distribution will be of the form below

$$f(E) \sim \exp\left(-\frac{E}{W}\right)\left[1-\frac{\overline{E_i}\left(\frac{E}{W}\right)}{\overline{E_i}\left(\frac{E_0}{W}\right)}\right] \tag{18}$$

where $W \equiv kT_e$ is the electron energy, $\overline{E_i}$ is the transient energy of the carrier, and E_0, the energy of impact ionization at threshold, is about 1.5 times of the silicon band-gap energy E_g. Beyond the threshold energy, avalanche process with visible light emission from the reverse-biased p-n junctions will be observed. In result, Eq. (18) can be reduced to be

$$f(E) \sim \exp\left(-\frac{E}{kT_e}\right) \tag{19}$$

which is a quasi-Maxwell's distribution that is similar to the energy distribution function of photon intensity if the photon-emission mechanism is simply assumed to be Bremsstrahlung radiation only. On the other hand, the distribution of hot-carrier can be expressed in terms of the acoustic phonon which assists electron-hole recombination in the indirect interband transition process mentioned previously because the energy of hot-carrier can be expressed as

$$E = (kT_e)\left(\frac{3\pi\mu_0 \mathrm{E}}{8s^2}\right) \tag{20}$$

where μ_0 is the mobility, E is the electric field, and s is the sound speed. Substituting Eq. (20) into Eq. (19), it follows that

$$f(E) \sim \exp\left(\frac{3\pi\mu_0 \mathrm{E}}{8s^2}\right) \tag{21}$$

According to the correlation between the effective temperature T_e and the mean-free-path λ_m and the correlation between the sound speed and the energy of phonon, the electron energy $W \equiv kT_e$ becomes

$$W = \frac{(q\mathrm{E}\lambda_m)^2}{3(1-\cos\theta)E_{phonon}} \tag{22}$$

where E_{phonon} is the longitudinal acoustic phonon energy.

Multiplying Eq. (14), Eq. (15), Eq. (18), and Eq. (22), the final predicted rate of photon-emission with the evidence of the absorption of photons by silicon itself being taken into account is obtained in the form below

$$R_s = R_0(h\nu)\exp\left[-\alpha(h\nu)X_j\right] \tag{23}$$

where X_j is the junction depth, and R_0 is the rate of photon-emission at the beginning without any absorption. Assuming the assistance of phonon in the indirect recombination is taken into account, the absorption coefficient $\alpha(h\nu)$, which is temperature dependent, for a given wavelength (or frequency ν) is given by

$$\alpha(h\nu) = C_1\left[\frac{(h\nu - E_g + E_{phonon})^2}{\exp\left(\frac{E_{phonon}}{kT_e}\right)} + \frac{(h\nu - E_g - E_{phonon})^2}{1-\exp\left(-\frac{E_{phonon}}{kT_e}\right)}\right] \tag{24}$$

where C_1 is a constant factor that is equal to the value of $\alpha(h\nu)$ at the effective temperature $T_e = 300K$. In addition, the temperature dependence on the band-gap energy E_g can be expressed as

$$E_g(T_e) = E_g(0) - \frac{aT_e^2}{b+T_e} \tag{25}$$

where $E_g(0)$ is the gap energy at 0 K, a and b are both constants related to the properties of silicon, and T_e is the absolutely effective temperature.

In summary, the new form of the photon-emission rate obtained by substituting the combination of Eq. (24) and Eq. (25) into Eq. (23) is a reasonable model of the combination of the indirect transition and direct transition that can be used to analyze the silicon light emission under

breakdown condition [24].

4. Conclusions

This study demonstrates a silicon light-emitting-device (LED) with a configuration that is similar to the PMOSFET (p-type metal-oxide-semiconductor field-effect-transistor) and that can be manufactured in a commercial foundry using the CMOS process according to the industrial standard. Photoluminescence and corresponding mechanisms are analyzed in detail. Moreover, because of very high flexibility of design, low production cost at large scale and monolithic integration with other components (e.g., waveguide and photo-detector), this silicon light source is one of the best choices of being used as the light source for optical interconnect application in modern optoelectronic CMOS integrated circuits [25].

Acknowledgements

This work is supported by the Open Foundation of Defense Key Disciplines Lab of Novel Micro-nano Devices and System Technology (Chongqing University, China), Project No.106112014CDJZR160001 supported by the Fundamental Research Funds for the Central Universities, the Open Foundation of State Key Laboratory of Electronic Thin Films and Integrated Devices under Contract KFJJ201508, the Science and Technology on Analog Integrated Circuits Laboratory under Contract 9140C090112150C09047, the Scientific Research Foundation for the Returned Overseas Chinese Scholars, Ministry of Education, China, the Chinese Fundamental Research Funds for the Central Universities under Contract ZYGX2015KYQD009, and the funding of Integrated Nanosystems Research Facility (INRF) and Calit2 in Irvine, CA.

References

[1] L. Khriachtchev, “Silicon Nanophotonics: Basic Principles, Present Status and Perspectives,” Pan Stanford Publishing, Singapore, 2008
[2] R. Newman, Phys. Rev., **100**(2), 700 (1955).
[3] A. Chynoweth, H. Mckay, Phys. Rev., **102(**2), 369 (1956).
[4] M. du Plessis, H. Aharoni, L. Snyman, Opt. Mater., **27**(5), 1059 (2005).
[5] H. Aharoni, M. du Plessis, IEEE J. Quantum. Electron., **40(**5), 557 (2004).
[6] M. duPlessis, H. Aharoni, L. Snyman, Sens. Actuator, A, **80(**3), 242 (2000).
[7] K. Xu, G. Li, IEEE Photon. J., **4**(6), 2159 (2012).
[8] K. Xu, J. Select. Topics Quantum Electron., **20(**4), 8201208 (2014).
[9] K. Xu et al., IEEE Trans. Electron. Dev., **61**(6), 2085 (2014).
[10] M. Lahbabi, M. Jorio, A. Ahaitoul, M. Fliyou, E. Abarkan, Mater. Sci. and Eng., **86**(1), 96 (2001).
[11] K. Xu, G. Li, J. Nanophoton., **7(**1), 073082 (2013).
[12] M. Herzog, F. Koch, Appl. Phys. Lett., **53(**26), 2620 (1988).
[13] J. Bude, N. Sano, and A. Yoshii, Phys. Rev. B, **45**, 5848 (1992).
[14] A. Obeidat, Z. Kalayjian, A. Andreou, and J. Khurgin, Appl. Phys. Lett., **70**(4), 470 (1997).
[15] K. Xu, G. Li, J. Appl. Phys., **113**, 103106 (2013).
[16] H. Ghazi, A. Jorio, I. Zorkani, Opt. Commun., **281**(12), 3320 (2008).
[17] M. Lahbabi, A. Ahaitouf, E. Abarkan, M. Fliyou, A. Hoffmann, J. Charles, B. Bhuva, S. Kerns, D. Kerns, Appl. Phys. Lett., **77**(20), 3182 (2000).
[18] S. Tam, P. Ko, C. Hu, “IEEE Trans. Electron Dev., **31(**9), 1116 (1984).
[19] L. Snyman, K. Xu, J. Polleux, K. Ogudo, C. Viana, IEEE J. Quantum Electron., **51**(6), 3200110 (2015).
[20] A. Lacaita, F. Zappa, S. Bigliardi, M. Manfredi, IEEE Trans. Electron. Dev., **40**(3), 577 (1993).
[21] K. Xu. H. Liu, Z. Zhang, Appl. Opt., **54**(21), 6420 (2015).
[22] K. Xu, Q. Yu, G. Li, IEEE J. Quantum Electron., **51**(8), 300106 (2015).
[23] K. Xu, S. Liu, J. Zhao, W. Sun, G. Li, Opt. Eng., **54**(5), 057104 (2015).
[24] K. Xu, “Hot carrier luminescence in silicon metal oxide semiconductor field effect transistor,” in Advances in Optoelectronics Research, Nova Science Publisher Inc., New York, pp. 1-28, 2014
[25] K. Xu et al., “Silicon avalanche based light emitting diodes and their potential integration into CMOS and RF integrated circuit technology,” in Adv. in Opt. Comm., Intech, Chapter 5, pp. 115-142, 2014

*Corresponding author: kaikaix@uestc.edu.cn